Conducting-State Properties of the KcsA Potassium Channel from Molecular and Brownian Dynamics Simulations

Shin-Ho Chung,* Toby W. Allen,* and Serdar Kuyucak†

*Department of Physics, Faculty of Sciences, and †Department of Theoretical Physics, Research School of Physical Sciences, Australian National University, Canberra, ACT 0200, Australia

ABSTRACT The mechanisms underlying transport of ions across the potassium channel are examined using electrostatic calculations and three-dimensional Brownian dynamics simulations. We first build open-state configurations of the channel with molecular dynamics simulations, by pulling the transmembrane helices outward until the channel attains the desired interior radius. To gain insights into ion permeation, we construct potential energy profiles experienced by an ion traversing the channel in the presence of other resident ions. These profiles reveal that in the absence of an applied field the channel accommodates three potassium ions in a stable equilibrium, two in the selectivity filter and one in the central cavity. In the presence of a driving potential, this three-ion state becomes unstable, and ion permeation across the channel is observed. These qualitative explanations are confirmed by the results of three-dimensional Brownian dynamics simulations. We find that the channel conducts when the ionizable residues near the extracellular entrance are fully charged and those near the intracellular side are partially charged. The conductance increases steeply as the radius of the intracellular mouth of the channel is increased from 2 Å to 5 Å. Our simulation results reproduce several experimental observations, including the current-voltage curves, conductance-concentration relationships, and outward rectification of currents.

INTRODUCTION

With the recent determination of the crystal structure of the KcsA potassium channel (Doyle et al., 1998), the focus of theoretical studies of ion permeation has shifted from gramicidin A to KcsA. So far, the main thrust of these studies has been to employ the atomic structure of the channel in molecular dynamics (MD) simulations to investigate permeation properties such as ion binding sites, selectivity, and diffusion (Guidoni et al., 1999, 2000; Allen et al., 1999, 2000a,b; Bernèche and Roux, 2000; Roux et al., 2000; Åqvist and Luzhkov, 2000; Luzhkov and Åqvist, 2001; Shrivastava and Sansom, 2000; Biggin et al., 2001). Although these MD-based investigations have given useful insights about the function of the KcsA channel, they are limited to the nanosecond time regime and therefore cannot predict the channel currents that require microsecond-long simulations. Because conductance is the main physiological observable characteristic of a channel, it is essential to devise a method that enables its computation. Using a simplified KcsA channel, we have shown in a previous article that three-dimensional Brownian dynamics (BD) simulations can fulfill this task (Chung et al., 1999). The shape of the model channel used in that work resembled that deduced from crystallography, but atoms constituting the channel were represented as a homogeneous, low-dielectric medium with a smooth water-protein boundary. This simplified model was a first step in BD studies of the KcsA channel, and it has provided considerable insight into permeation process in multiple-ion channels. The next step is to incorporate the full structural information obtained from crystallography into BD simulations, so that channel function can be directly related to the structure of the KcsA protein. Here we carry out BD simulations on a potassium channel model that includes all the experimentally determined channel protein, composed of 396 residues and 3504 atoms excluding polar hydrogens.

Paramagnetic spin resonance studies (Perozo et al., 1998, 1999), associated with the pH-dependent gating of this channel (Heginbotham et al., 1999; Cuello et al., 1998), have indicated that the experimental structure corresponds to a closed conduction state and that the transmembrane helices forming the intracellular pore move away from the channel axis during gating. Also, in the crystal structure, the radius of the narrowest section of the pore on the intracellular side is ~1.2 Å, smaller than the radius of the potassium ion (1.33 Å). We therefore first modify the intracellular entrance of the channel with MD simulations to create a set of possible open-state structures. To gain insight into the permeation mechanism, we construct potential energy profiles experienced by an ion traversing the channel that is occupied by other ions. These multi-ion profiles reveal equilibrium ion positions, the effect of charges on ionizable residues required for the channel to conduct, and the rate-limiting step for ions passing the channel. To quantify these predictions, we perform BD simulations, employing various findings from atomic detail MD calculations, namely, ionic diffusion estimates and ionic potential of mean force interactions. By carrying out these simulations we observe the combined effects of gate size and charge distribution on channel conductance, propose a conducting-state channel based on MD simulations with the full channel protein, and

Submitted June 18, 2001, and accepted for publication October 29, 2001.

Address reprint requests to Dr. S. H. Chung, Department of Physics, Faculty of Sciences, Australian National University, Canberra, ACT 0200, Australia. Tel.: 61-2-6125-2024; Fax: 61-2-6247-2792; E-mail: shin-ho.chung@anu.edu.au.

0006-3495/02/02/628/18 $2.00

improve our understanding of permeation in multiple-ion channels.

METHODS

We employ a combination of fully microscopic MD and semi-microscopic BD simulations to provide connections between the known atomic structure of the KcsA potassium channel and its observable properties. First we describe our methods for generating possible open-state structures with MD and then present our BD technique.

Molecular dynamics: creating an open state

We increase the radius of the intracellular gate in a series of MD simulations, with the CHARMM v.25 package (Brooks et al., 1983), to produce a set of conducting channel candidates to be tested with BD. During MD simulations, the protein is kept neutral (Lazaridis and Karplus, 1999) and the CHARMM 19 extended atom parameter set is employed. The experimental KcsA protein structure (Doyle et al., 1998), taken from structure file 1BL8 of the Protein Data Bank, is modified to include terminal residues and missing side chains, as described previously (Allen et al., 2000a). The structure is then hydrated with SPC/E water molecules and attached to intracellular and extracellular reservoirs of water. Constraints representing the interactions of the protein with a membrane layer are included so that the protein undergoes no large distortions while ion selectivity is unaffected (Allen et al., 2000a). Following 200 ps of equilibration, three potassium ions are placed near the experimentally determined positions, based on Rb^+ difference maps (Doyle et al., 1998), and held with 100 $kT/Å^2$ harmonic constraints (1 $kT = 4.11 \times 10^{-21}$ J at $T = 298$ K). The ions are placed inside the wide cavity, near the T_{75} carbonyl oxygen (a broad maximum in charge density), and near the Y_{78} carbonyl oxygen. BD simulations, described in Results, show that an ion always resides near the intracellular entrance of the channel due to the presence of glutamic acid residues. Because the presence of a potassium ion will polarize the protein, we also hold an ion in this region during MD simulations.

In BD simulations, the channel protein is assumed to have a rigid structure corresponding to the average positions of atoms forming it. Because the selectivity filter is quite narrow and contains two ions, it is likely to exhibit sizable fluctuations during MD simulations. Therefore, we impose some uniformity on the filter protein by applying a cylindrical harmonic potential (100 $kT/Å^2$) to carbonyl oxygen atoms (residues 75–78) so as to maintain a pore radius of ~1.4 Å. This filter radius is similar to that observed in the crystallographic structure (Doyle et al., 1998), and the overall change to the shape of the filter segment is minimal. Despite this necessary simplification imposed on the model, BD captures the salient conduction properties of potassium channels. This is because the most essential features that govern the permeation of ions across a narrow pore are captured in our model. These are the overall channel shape, the magnitude of charges that creates an energy well deep enough to attract three ions in and in the vicinity of the selectivity filter, the radius of the intracellular gate, and the charges placed on the ionizable residues guarding the entrances. There are small details that can be neglected in the model for the purpose of BD simulations. For example, small variations in the radius of the filter have no perceptible effects on electrostatic calculations and BD results. In contrast, such variations would have a drastic effect on MD results. We also note that the outermost of the two resident ions is ejected from the filter ballistically and almost instantaneously (see, for example, Allen et al., 1999) when the stable equilibrium is disrupted by a third ion penetrating the filter. Thus, the motions of the carbonyl oxygens lining the filter owing to the rapid movement of potassium ions through the conduit will make no difference on the macroscopic properties deduced from BD simulations.

Initially, atomic constraints of 20 $kT/Å^2$ are applied to the α-carbon atoms in the inner and outer helices. In a series of 100-ps simulations, the target restraints for $z < 0$ Å are moved away from the channel axis in small steps until the minimum radius of the intracellular pore reaches the desired value. Intracellular gates of approximate minimum radii $R_{min} = 2$, 3, 4, and 5 Å are generated with this procedure. All target restraints on the inner and outer helices are then removed and a repulsive cylinder is placed inside the intracellular pore such that any atom whose center resides within $z < 0$ Å and $r < R + 2$ Å will experience a harmonic potential (200 $kT/Å^2$). This leaves both the inner and outer helices free to rotate and reach a minimum in the potential surface for this widened structure. It has been suggested that rotation of the transmembrane helices occurs during gating (Perozo et al., 1998, 1999). However, because this evidence is only qualitative, such modifications to the structure have not been imposed during modeling. Also, because the channel is widened by a maximum of ~4 Å, rotation of helices is expected to be small. Simulation with the transmembrane helices released is carried out for an additional 50 ps during which little change in the pore shape occurs because of the placement of the repulsive cylinder. A sample from the trajectory is taken that maximizes the current in BD simulations. Water molecules and ions are discarded and a single subunit is chosen and replicated to impose fourfold symmetry about the channel axis.

Fig. 1 *A* illustrates the KcsA potassium channel protein structure for an open-state channel with the minimum intracellular gate radius of $R_{min} = 3$ Å, hydrated with SPC/E water molecules. For clarity, we show only two of the four subunits that form the pore. The dielectric interface between protein and water is determined by assigning the protein atoms Born radii (Nina et al., 1997) and tracing the channel pore with a water molecule sphere of radius 1.4 Å. The profile obtained from the minimum boundary radius at each axial position is rotated around the channel axis by 360° (Fig. 1 *B*) to generate a three-dimensional pore. Finally this axially symmetrical pore shape is superimposed on the protein structure. Because of the fourfold symmetry of KcsA, and the large size of the water molecule in comparison to the size of the KcsA pore, the axially symmetric boundary is found to be a good approximation. For the model system illustrated in Fig. 1 *B*, the boundary has an intracellular pore ($-23 \le z < -3$ Å) with radius ≥ 3 Å, reaching a maximum of 5.5 Å in the cavity region ($-3 \le z < 8$ Å), whereas that in the selectivity filter ($8 \le z \le 23$ Å) is $\ge$1.4 Å. The total length of the channel, including the inner and outer vestibules, is 68 Å. When performing BD simulations, cylindrical reservoirs are attached to the channel ends as shown in Fig. 1 *C*. Because the reservoirs in our system extend only a short way from the pore, it is the channel protein itself that is forming the dielectric boundary, and not a lipid bilayer. Thus the thickness of the low dielectric slab is larger than that of a typical membrane. The origin ($z = 0$) is chosen to lie near the center of the wide cavity region. We refer to Doyle et al. (1998) for a guide to the positions of each residue within the KcsA protein structure.

The widening of the intracellular pore by spreading of transmembrane helices is evident in Fig. 2, where pore radius profiles of open-state models with $R_{min} = 3$, 4, and 5 Å are compared with that of the crystallographic structure (broken line). We note that these curves are calculated with the use of atomic Born radii of protein atoms (Nina et al., 1997), and not van der Waals radii. As a result the crystallographic structure has a pore radius as small as 0.6 Å in the intracellular gate region. Rotation of the helices around axes parallel to the z axis during modeling of the $R_{min} = 3$ Å channel never exceed 5°. The axes chosen for this measurement, for the inner and outer helices, pass through the C_{90} and A_{50} α-carbon atoms, respectively.

Brownian dynamics simulations

We perform three-dimensional BD simulations to predict the channel conductance. The method of implementing BD simulations is detailed elsewhere (Li et al., 1998; Chung et al., 1998, 1999). Here we give a brief description of the method and refer to our previous publications for further

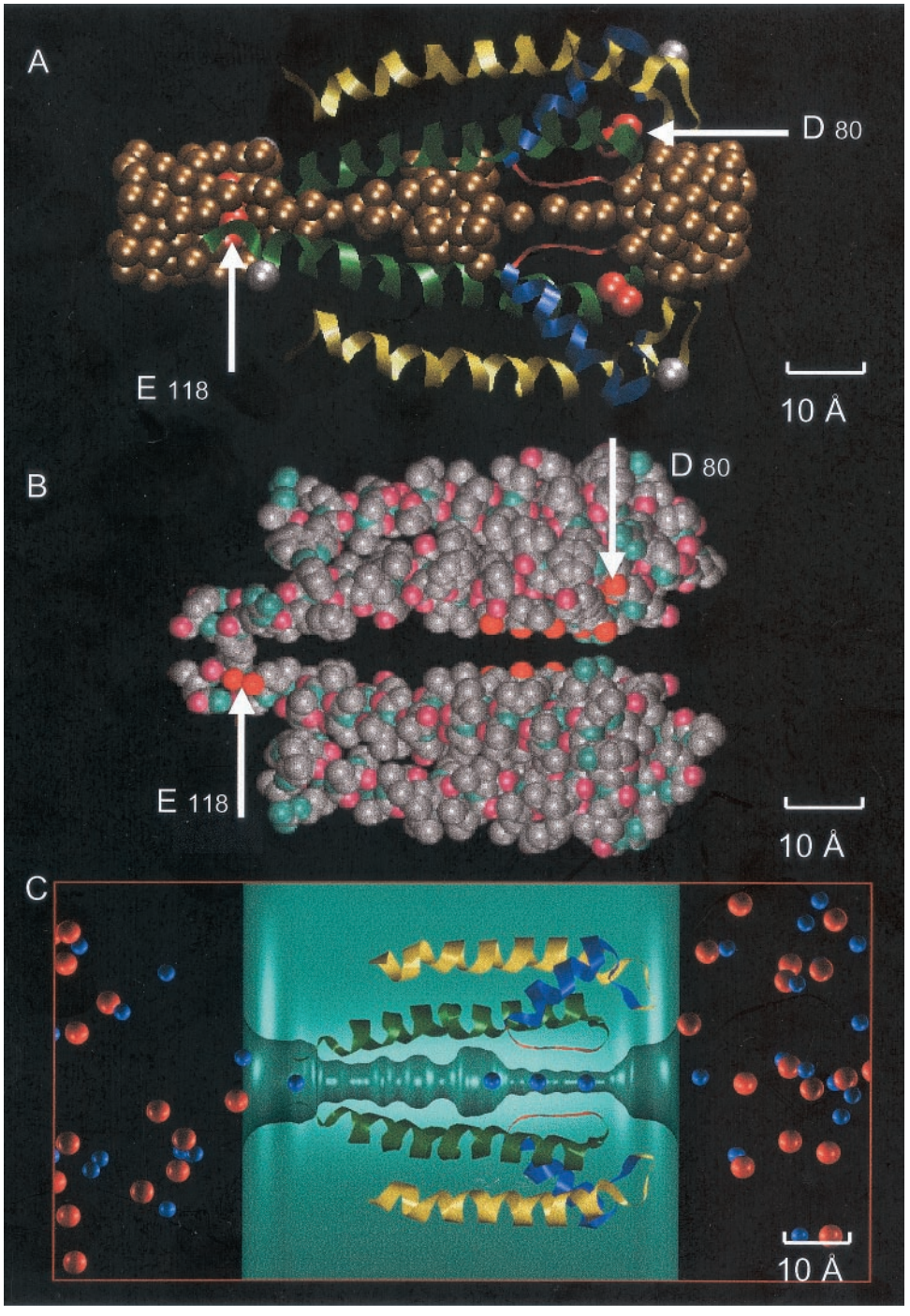

FIGURE 1 Model potassium channel. (*A*) Two of the four subunits of the full experimentally determined protein and the positions of water molecules inside of the pore are illustrated. The aspartate-arginine pairs near the extracellular entrance of the channel (*right-hand side*) and the glutamate-arginine pair nears near the intracellular entrance of the channel are indicated in red and silver. (*B*) An outline of the water-protein boundary of a channel with the minimum intra-pore radius of R_{min} = 3 Å is shown. The boundary is first smoothed with a water molecule, and then the curve is rotated by 360° to obtain a three-dimensional channel structure. (*C*) For BD simulations, a reservoir of 30-Å radius is attached at each end of the channel and a fixed number of potassium and chloride ions are placed in each reservoir. The height of the reservoir is adjusted to obtain a desired ionic concentration.

details. In BD simulations, the trajectories of ions are followed by integrating the Langevin equation:

$$m_i \frac{d\mathbf{v}_i}{dt} = -m_i\gamma_i\mathbf{v}_i + \mathbf{F}_{Ri} + q_i\mathbf{E}_i + \mathbf{F}_{Si}, \qquad (1)$$

where m_i, $\mathbf{v}_i$, $m_i\gamma_i$ and q_i are the mass, velocity, friction coefficient, and charge of an ion with index *i*. The quantities $\mathbf{F}_{Ri}$, $\mathbf{E}_i$, and $\mathbf{F}_{Si}$ are the random force, systematic electric field, and short-range force experienced by the ion, respectively. Electrostatic forces are determined by solving Poisson's equation with the boundary element method (Hoyles et al., 1996, 1998b) and implemented in BD simulations using look-up table techniques (Hoyles et al., 1998a).

The Langevin equation (Eq. 1) is solved using the algorithm of van Gunsteren and Berendsen (1982). A multiple time-step algorithm is used, where a time-step of Δt = 100 fs is employed in the reservoirs and 2 fs in the channel. The latter is necessitated by the fact that forces change rapidly inside the channel. Recalling that the relaxation time constant, γ^{-1}, is 31 ps for potassium ions, their motion corresponds to over-damped diffusion in the reservoirs ($\Delta t \gg \gamma^{-1}$) but not in the channel. A temperature of 298 K is assumed throughout. The friction coefficient $m_i\gamma_i$ in Eq. 1 is related to the diffusion coefficient D_i by the Einstein relation $D_i = kT/m_i\gamma_i$. Bulk

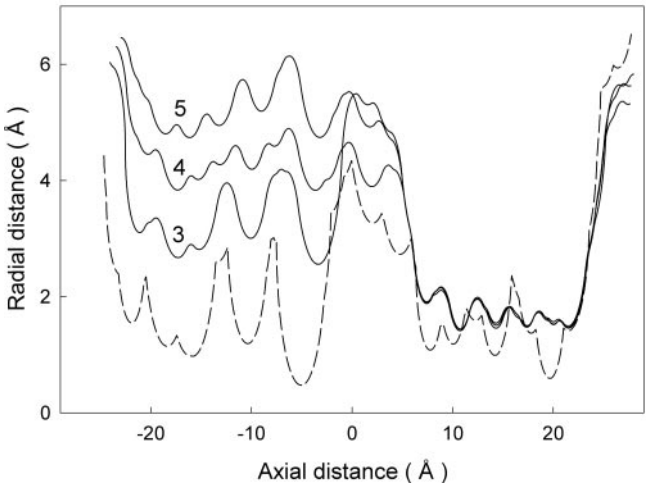

FIGURE 2 Pore radius profiles of four different open-state channels and that of the crystallographic structure (— — —). The numbers accompanying the traces are the minimum pore radii (R_{min}) of the entrance from the intracellular side. Pore radii of R_{min} = 3, 4, and 5 Å are shown, whereas the channel with R_{min} = 2 Å has been omitted for clarity.

ionic diffusion coefficients (1.96×10^{-9} m^2/s and 2.03×10^{-9} m^2/s for K and Cl ions, respectively (Lide, 1994)) are employed in reservoirs, but reduced values are used in the channel according to the MD results (Allen et al., 2000b). Within the intracellular pore, we maintain a bulk diffusion coefficient for the K ion, whereas a value of 50% bulk diffusion is employed in the hydrophobic cavity region. Because the value of the diffusion coefficient used in the selectivity filter has been shown to have little effect on channel conductance (Chung et al., 1999), we also use a value of 50% bulk in that region.

The dielectric constant of the protein is assumed to be $\varepsilon p = 2$ in the main body of this work, though we do consider the effect of small variations (2–5) on the results. The situation with regard to the channel water is less certain. It is expected that the dielectric constant of the channel water will be reduced from its bulk value of 80 (Sansom et al., 1997), but the amount of reduction is highly dependent on the process one uses. For example, the response of water molecules to an external perturbation is highly suppressed, so this type of calculation would result in a very low ε value. On the other hand, if one considers dielectric screening of an ion, a much larger ε value is expected because the potassium ions appear to be well solvated throughout the channel (Allen et al., 1999, 2000a). In past simulations on a model KcsA channel (Chung et al., 1999), a value of 60 was found to optimize conductance, which we adopt here as well. Because the boundary element method does not permit ions to cross dielectric boundaries, a uniform dielectric constant of 60 is employed throughout channel and bath water. The change from reservoir (80) to channel water (60) is represented by a Born energy barrier of

$$E_B = \frac{q^2}{8\pi\varepsilon_0 R_B}\left(\frac{1}{60} - \frac{1}{80}\right) \approx 0.6\ kT, \qquad (2)$$

which assumes a Born radius of R_B = 1.93 Å, determined from the enthalpy of hydration for K^+ ions (Bockris and Reddy, 1970). This barrier is introduced as a smooth switching function erected at the channel entrances (Chung et al., 1999). The short time-step of 2 fs used in the channel pore ($-25 \le z \le 25$ Å) ensures that ions are subjected to these short-ranged forces. Ions also interact with the channel protein lining via a repulsive short-range potential similar to that described in Chung et al. (1999). The Coulomb interaction between ions is modified at short distances by strongly repulsive contact, weakly attractive dispersion, and oscillating hydration forces. A correct modeling of these short-range contributions is very important in multi-ion channels because they have a direct bearing on the relative positions of ions within the channel. This has been highlighted in recent MD simulations of the KcsA channel that revealed the role played by hydration waters in positioning of ions in the selectivity filter (see, for example, Åqvist and Luzhkov, 2000; Allen et al., 2000a; Bernèche and Roux, 2000). We have previously incorporated these short-range ion-ion interactions in BD simulations by parameterizing the potentials of mean force obtained from MD simulations (Corry et al., 2001). We adopt the same analytical form here:

$$U_S^{\text{ion-ion}}(r) = U_0\{(R_c/r)^9 - \exp[(R - r)/c_e] \times \cos[2\pi(R - r)/c_w]\}, \qquad (3)$$

where U_0 is the strength of the potential, R_c is the contact distance defining the repulsive first term. The second term describes the damped oscillations due to hydration forces with $R \approx R_c$, c_e = 1 Å, and c_w = 2.76 Å (water diameter). Table 1 lists the parameters for each ion pair.

TABLE 1 Parameters for the short-range ion-ion potential function of Eq. 3

Ions	U_0 (kT)	R_c (Å)	R (Å)
K-K	2.5	4.26	4.46
K-Cl	5.2	3.14	2.94
Cl-Cl	1.4	5.22	5.42

A cylindrical reservoir of 30-Å radius and variable length is connected to each end of the channel (see Fig. 1 *C*). We note here that the reservoir boundaries simply serve to confine the ions within the simulation system, thus maintaining the average concentrations in the baths at the desired values. Scattering of an ion from the boundary wall can be viewed as an ion moving out of the reservoir and another one entering at the same time. Implicit in the use of reservoirs is the assumption that electrolyte solution continues beyond its boundaries. Symmetric concentrations are generated with 16 potassium and 16 chloride ions in each reservoir, and the reservoir length is adjusted to set the concentration. With the exception of the current-concentration curves, 300 mM is used in all simulations, which corresponds to a reservoir length of 32 Å. During conduction events, the average concentration in the reservoirs is maintained with a stochastic boundary (Chung et al., 1999).

In experiments, a potential difference is applied via electrodes at macroscopic distances from the channel. In a small system such as the one used in BD simulations, this procedure cannot be simply mimicked by fixing the potential at the boundaries. Because the channel is highly charged, this would distort the potential in the channel vicinity compared with the experimental set-up. To circumvent this problem, we generate the potential difference across the channel via a uniform applied electric field of strength E_0. Operationally, this is equivalent to having a pair of isopotential plates located at large distances from the channel. In the absence of any dielectric boundary, the potential difference across a channel of length l would be simply lE_0. The presence of a dielectric boundary and charges on the protein wall, however, distorts this field in and nearby the channel. Thus, the precise potential difference across the channel depends on the selected reference points at the two sides of the potassium channel. A convenient choice for our purposes is the center of each reservoir at $z = \pm 50$ Å, which we employ throughout this work. To determine the potential difference across the reference points, we measure sample potentials along the z axis once every 10 ps and average over the simulation period with 300 mM KCl in the reservoirs. The difference in the average potentials between the reference points, ΔV, is taken to be the potential difference across the channel. In the following, unless otherwise stated, we apply an electric field of strength $E_0 = 2 \times 10^7$ V/m in BD simulations. The corresponding values of ΔV for each channel are given in Table 2. Note that because of

TABLE 2 Potential differences between the reservoir centers due to applied electric fields of $\pm E_0$ for channels with radii R_{min} = 2, 3, 4, and 5 Å

R_{min} (Å)	$\Delta V(+E_0)$	$\Delta V(-E_0)$
2	252	−284
3	247	−269
4	221	−278
5	220	−265

Here ΔV is in mV and $E_0 = 2 \times 10^7$ V/m throughout.

the highly asymmetric charge distribution in the KcsA channel, the ΔV values are not symmetric.

The energy profile of an ion along the z axis is constructed by solving Poisson's equation with a test ion fixed at regular positions along the channel axis. The energy profile seen by an ion entering the channel already housing one or more cations is found using a steepest-descent algorithm (Chung et al., 1999), where forces on all resident ions are minimized and the total energy of the system is recorded at each test ion position.

The BD program is written in FORTRAN, vectorized, and executed on a supercomputer (Fujitsu VPP-300). The amount of vectorization varies from 67% to 92%, depending on the number of ions in the reservoirs. With 64 ions in the reservoirs, the CPU time needed to complete a simulation period of 1 μs is ~53 h. Simulations under various conditions, each lasting 1×10^6 time steps (0.1 μs), are repeated 10–30 times.

RESULTS AND DISCUSSION

Charges on ionizable residues

The KcsA sequence (Doyle et al., 1998) consists of a number of ionizable residues close to the permeation pathway that may affect channel conduction. These residues, and their approximate positions, are listed in Table 3. Our model channel is taken to be overall neutral by grouping ionizable residues into likely dipoles. The presence of any net local charge severely hampers ion permeation, presumably due to the low dielectric strength of the protein. As shown in Table 3, there is only one unpaired arginine residue R_{27} in the protein sequence. This residue is taken to be neutral in our model because it is found to have a strong destabilizing influence on permeating ions in this sector of the channel (Allen et al., 2000a). We stress that R_{27} is in a region where 21 residues from the N-terminus and 39 residues from the C-terminus are missing from the experimental KcsA sequence, and also it is in close proximity to the lipid bilayer surface. Therefore, it is reasonable to assume that R_{27} could be neutralized by missing charged residues or ions in solution.

TABLE 3 Radial and axial positions (r, z) in units of Å of ionizable residues in the modified KcsA channel with R_{min} = 3 Å

Acid	Base	Charge
E_{51} (15.7, 24.2),	R_{52} (25.4, 23.1)	0
D_{80} (7.1, 20.7),	R_{64} (14.0, 22.4)	q_e
E_{71} (7.0, 17.1),	R_{89} (16.8, 18.6)	0
	R_{27} (20.6, −15.0)	0
E_{118} (4.5, −21.1),	R_{117} (16.9, −18.0)	q_i

Positions of the closest carboxyl oxygen to the axis on glutamic acid (E) and aspartic acid (D) residues and of the guanidine carbon on arginine (R) residues are provided. The last column indicates the charge modulus assigned to these residues.

The E_{51}/R_{52} pair is far from the channel axis and has been found to have little impact on conduction. These residues are therefore kept neutral. For reasons to be discussed below, the E_{71}/R_{89} pair are also kept uncharged in our simulations. The remaining ionizable residues D_{80}/R_{64} and E_{118}/R_{117} are required to be charged for the channel to conduct. We have examined the influence of these dipoles on the conductance properties of the R_{min} = 3 Å channel by performing BD simulations. We assign charges $-q_e$ and $+q_e$ on the D_{80}/R_{64} pair near the extracellular side, creating four mouth dipoles. Similarly, charges $-q_i$ and $+q_i$ are placed on E_{118}/R_{117} residues to create four intracellular mouth dipoles. These charges are distributed among the atoms of ionizable side chains, following the method described by Lazaridis and Karplus (1999), and have been indicated in Fig. 1, *A* and *B*. Both set of dipoles provide attractive energy wells for cations to enter the pore and prevent anions from entering it. Analysis of MD trajectories reveals that the fourfold symmetry of the E_{118} side chains is maintained in the presence of an ion in the vicinity of these residues. Thus the rigid tetramer employed in BD simulations is appropriate and does not introduce an artificially deep energy well at the intracellular entrance.

We show in Fig. 3 the variation in outward (filled circles) and inward (open circles) channel currents with charge q_i on intracellular dipoles (Fig. 3 *A*) and q_e on extracellular dipoles (Fig. 3 *B*). The positions of these polar residues are indicated in the inset as dark and white balls. Electric fields of $+E_0$ and $-E_0$ are applied to generate the outward and inward currents, respectively (see Table 2 for the corresponding potential differences). The charge q_e is fixed at $0.9e$ during optimization of q_i, whereas q_i is fixed at 0.7 e during optimization of q_e. When q_i is instead held at 0.3 e during optimization of q_e, very similar outward flowing currents are observed, as shown in Fig. 3 *B* (gray triangles). Both outward and inward currents increase rapidly with q_i and remain high between $q_i = 0.3\,e$ and $0.8\,e$ (Fig. 3 *A*). The current declines slightly when the charge is further increased to $0.9\,e$. In contrast, both outward and inward currents reach a maximum when q_e is near the full unit charge e (Fig. 3 *B*). A small deviation in q_e is seen to cause a rapid decline in the channel current.

Fig. 4 shows the variation of outward (filled circles) and inward (open circles) currents with charge q_i on the intracellular dipoles for the channels with R_{min} = 2, 4, and 5 Å (*A*, *B*, and *C*). The relative magnitude of the current is seen to be sensitive to q_i for R_{min} = 2 Å, but this dependence is much less pronounced for the larger channels with R_{min} = 4 or 5 Å. The curves for optimization of q_e show similar

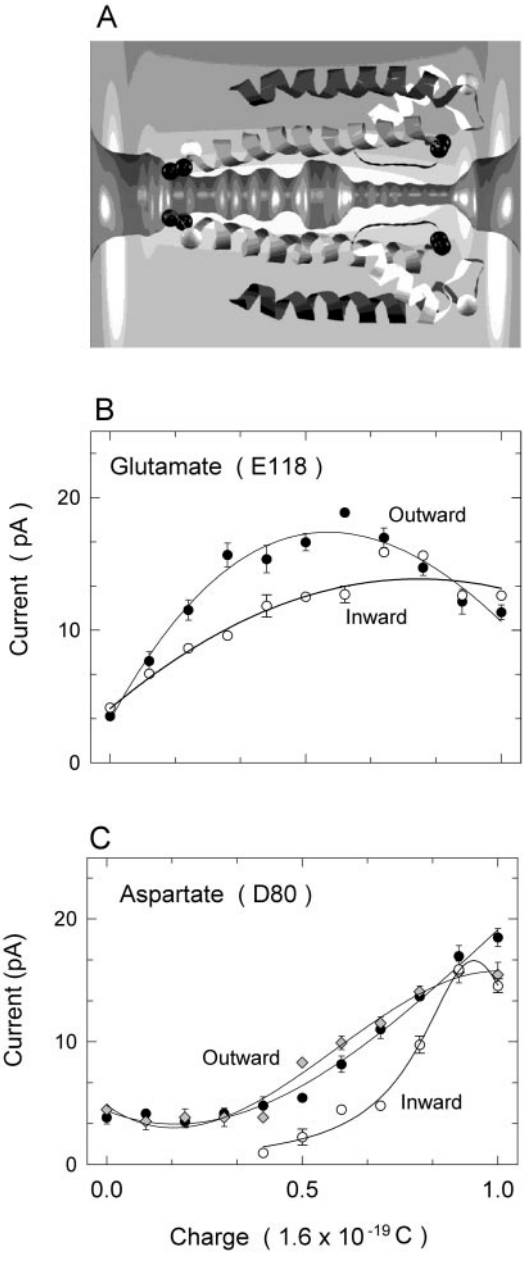

FIGURE 3 Dependence of channel current on fixed charge strengths for channel with R_{min} = 3 Å. (*A*) The current passing through the channel under a driving field of E_0 (●) or $-E_0$ (○) is plotted against the charge q_i on each of the four glutamate (E_{118}) and arginine (R_{117}) pairs. The charge on each of the four aspartate (D_{80}) and arginine (R_{64}) pairs are held constant at 0.9 *e* during the optimization of q_i. (*B*) Same as in *A* but against the charge q_e on each of the four aspartate (D_{80}) and arginine (R_{64}) pairs. The charge q_i is fixed at 0.7 *e* during optimization of q_e. Similar results are obtained when the charge q_i is fixed at 0.3 *e* during optimization of q_e, with the outward current shown as gray triangles. In this and all subsequent figures, a data point represents the average of 10–20 sets of simulations, each set lasting 1×10^6 time steps (or 0.1 μs). Error bars in this and following figures have a length of 1 SEM and are not shown when they are smaller than the data points.

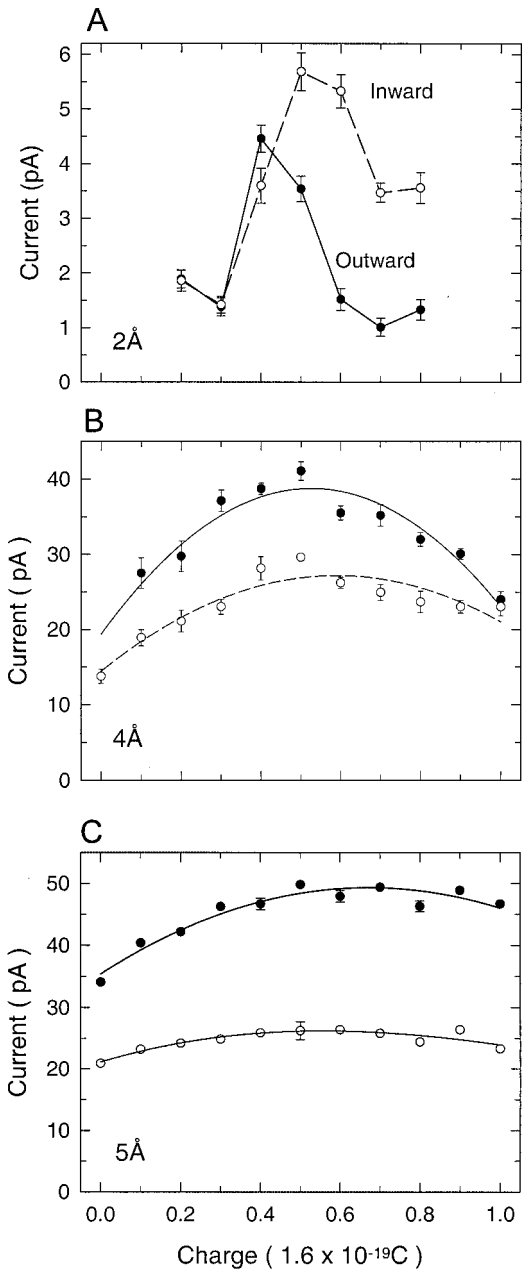

FIGURE 4 Dependence of channel current on fixed charge strengths and channel radius. The charge on the extracellular dipoles (D_{80}/R_{64}) are fixed at $q_e = e$ throughout. (*A*) The outward (●) and inward (○) currents across the channel with R_{min} = 2 Å under a driving field of $\pm E_0$, are plotted against the charge q_i on the intracellular dipoles (E_{118}/R_{117}). (*B*) Same as in *A* but for a channel with R_{min} = 4 Å. (*C*) Same as in *A* but for a channel with R_{min} = 5 Å.

trend as those illustrated in Fig. 3 *C*, suggesting use of full unit charges for optimal currents.

In the preceding series of simulations, the ionizable residues E_{71} and R_{89} are kept neutral. Despite the proximity of the E_{71} side chain to the selectivity filter, calculations have shown that it is energetically favorable for E_{71} to be pro-

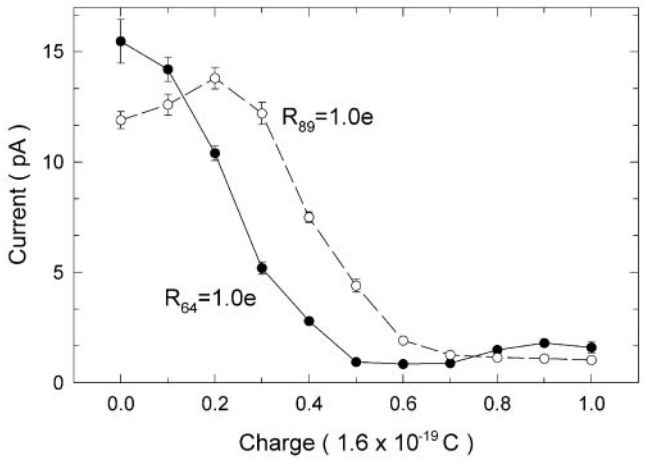

FIGURE 5 Variation of currents with the relative charge placed on the two ionizable residues (D_{80} and E_{71}) near the extracellular channel entrance for $R_{min} = 3$ Å. A fraction of the charge on D_{80} is transferred to E_{71}, and the current across the channel is determined. The total charge shared between the two residues is kept constant at $-e$. In one series of determinations, the full positive charge is placed on the R_{64} residue, while keeping the R_{89} residue neutral (●). The same series of simulations is carried out once again, placing the full positive charge on the R_{89} residue and keeping the R_{64} residue neutral (○).

tonated (Roux et al., 2000; Luzhkov and Åqvist, 2000). However, recent calculations have predicted that the presence of multiple cations can increase the probability of this residue being charged (Ranatunga et al., 2001). Here we examine the effect of placing charges on the E_{71} and R_{89} residues. First, we shift a fraction of the unit charge $-e$ on the D_{80} residue to the E_{71} residue (i.e., the proton on E_{71} spends a fraction of its time on D_{80}) and measure the current across the channel. This process is repeated until the full charge is transferred from one residue to the other. In this first series of simulations, the R_{64} residue is fully protonated, whereas residue R_{89} is in its neutral state. In Fig. 5, the current is plotted against the charge on the E_{71} residue (filled circles). When the full charge $-e$ is on the D_{80} residue, the outward current under the driving field of $+E_0$ is at a maximum. The current rapidly decreases as the charge is shifted from D_{80} to the E_{71} residue, reaching a minimum at halfway through and remaining at this 10% level thereafter. We repeat the same series of simulations with the full charge on R_{89} and no charge on the R_{64} residue. The outward current across the channel first increases slightly and then declines rapidly as the charge on the aspartate residue is gradually transferred from the D_{80} residue to the E_{71} residue (open circles in Fig. 5). With the positive charge shifted to R_{89}, the largest number of potassium ions are translocated when 0.2 *e* is placed on E_{71} and the remaining 0.8 *e* on the D_{80} residue. The current rapidly attenuates, as before, when the charge on the glutamate residue is further increased. We choose R_{64} protonated and R_{89} deprotonated to obtain the maximum current, as seen in Fig. 5. With both R_{64} and R_{89} protonated and both D_{80} and E_{71} carrying the full charge $-e$, the energy well in the pore becomes deep enough to attract on average 4.5 ions in the absence of an applied electric field. Although the system could be made to conduct, this observed number of resident ions in the filter and wide cavity is inconsistent with the crystallographic observations (Doyle et al., 1998). We thus assume that one of the arginine residues, possibly R_{89}, is locally neutralized by a foreign anionic species and only one charge is shared between D_{80} and E_{71}, but predominantly on the former in the conducting state.

We conclude from these results that a value of $0.9 \leq q_e \leq 1.0$ *e* for the D_{80} and R_{64} residues, and $0.3 \leq q_i \leq 0.8$ *e* for the E_{118} and R_{117} residues provide near optimal channel performance in both directions of permeation for $R_{min} = 3$ Å. Also, the E_{71} residue near the selectivity filter must be kept neutral for conduction to take place. In the following simulations, we consider two combinations of mouth dipoles with $q_i = 0.3$ and 0.7 *e* (the former value is assumed if not explicitly stated). For the 2-, 4-, and 5-Å channels, $q_i = 0.5$ *e* is used. The full unit charges are placed on the extracellular dipoles (D_{80} and R_{64}) throughout. We remark that the KcsA channel is usually closed at neutral pH but can remain in a conducting state at low intracellular pH (Heginbotham et al., 1999). Because the E_{118} side chains are in close proximity to the cytoplasmic side of the membrane and accessible to channel water, they are subject to protonation at low pH. We conjecture that the open state of the KcsA channel is likely to involve a reduced charge on the intracellular mouth dipole. Had we placed the full electronic charges on the glutamate and arginine residues guarding the entrance of the intracellular pore throughout, the outward current would have been reduced on average by 46% and the inward current by 26% from the values we report here.

Energy profiles

We illustrate in Fig. 6 *A* the potential energy of a potassium ion brought into the channel from the intracellular reservoir in the absence of other ions. The charge on the intracellular dipole is fixed at $q_i = 0.7$ *e*. Profiles with $q_i = 0.3$ *e* (not shown here) are similar to those illustrated in Fig. 6, except that the well near the intracellular entrance of the channel is shallower. The energy well experienced by a single ion is deep, reaching 67 *kT* within the selectivity filter with respect to the intracellular reservoir. Fig. 6 *B* shows the energy profile experienced by a second ion entering the channel already housing one ion. The position of the resident ion when the test ion reaches the center of the channel ($z = 0$ Å) is indicated as an upward arrow. In constructing this and subsequent profiles, we allow the resident ions in the channel to adjust their positions so that both axial and radial components of the force on them are minimized. Thus, the potential profile for multiple ion systems, calculated with a steepest-descent algorithm (Chung et al., 1999), corre-

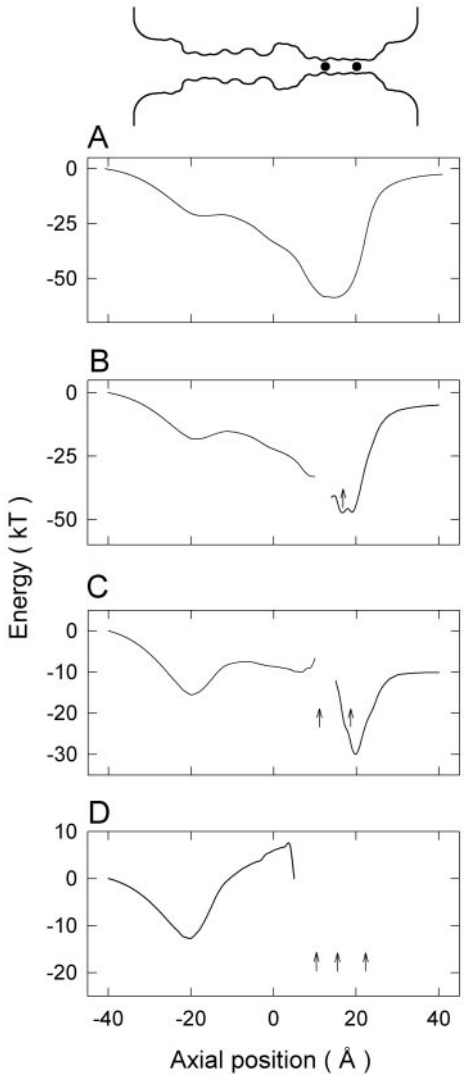

FIGURE 6 Electrostatic energy profile of an ion traversing the channel with R_{min} = 3 Å. The potential energy of a potassium ion is plotted in 1-Å intervals in the *z* direction with a driving field of $E_0/2$ (ΔV = 118 mV). The ion's *z* coordinate is fixed, but it is allowed to move to its minimum energy position in the *x-y* plane. In the absence of any resident ions in the channel, the test ion encounters a deep energy well of a depth of 67 *kT* at z = 13 Å (*A*). The energy profiles are constructed in the presence of 1 (*B*), 2 (*C*), and 3 (*D*) ions in the channel. The upward arrows indicate the location of the resident ions when the test ion is at the center of the channel (z = 0 Å). The schematic channel in the inset shows the positions of the ions in case *C*.

sponds to the total electrostatic energy required to bring in the charge on the test ion from an infinite distance in infinitesimal amounts. With two ions in the selectivity filter, a third ion entering the channel sees an energy well, created by the mouth dipoles near the intracellular entrance (Fig. 6 *C*). The ion needs to overcome a central barrier of 7–8 *kT* to move toward the wide cavity region. Once in the cavity, it experiences only a shallow energy well signifying the low stability of the three-ion system. A fourth ion entering the channel sees a small energy well and then a steeply rising energy barrier within the intracellular pore (Fig. 6 *D*). The three-ion equilibrium is disrupted when the fourth ion enters the pore, resulting in expelling of the outermost ion.

The electrostatic profiles constructed above ignore the influence of ionic atmosphere and other dynamic effects such as entropy. BD simulations indicate that anions do not enter the channel. Therefore, neglect of the counterions is justified, and one can still gain useful insights on the permeation process by examining the potential profiles in the channel. From the profiles illustrated in Fig. 6, it is clear that conduction will not take place unless there are two or three resident ions in the channel. For a single ion to traverse the selectivity filter, it has to gain an energy of nearly 60 *kT* to exit the energy well shown in Fig. 6 *A*. Similarly, the energy well seen by a second ion is ~40 *kT* (Fig. 6 *B*), also too deep to allow permeation. In the presence of two resident ions (Fig. 6 *C*), the third ion needs to overcome a smaller energy barrier of ~7–8 *kT*, when moving from the intracellular entrance up into the cavity. This is expected to be the rate-determining step for conduction. These suppositions are tested in the following sections using BD simulations.

Electric potential across the pore

It is of interest to determine the electric potential profile inside the channel during BD simulations. To construct such a profile, we measure once every 10 ps the electric potential along the *z* axis of the channel in 1-Å steps, and average over the simulation period. The average potential profiles created by applied electric fields of $+E_0$ (solid line) and $-E_0$ are depicted as solid curves in Fig. 7, *A* and *B*, respectively, for a channel with minimum gate radius 4 Å. The uniform electric field, which may be imagined to be generated by a pair of isopotential plates located at large distances, is distorted by the dielectric boundary. The potential differences generated between $z = \pm 50$ Å by these two applied electric fields are listed in Table 2. As mentioned in Methods, we take the measured potentials in plotting the current-voltage curves (see later). Inside the pore, the potential does not change linearly; instead, it fluctuates wildly owing to the presence of the fixed charges on the protein wall and resident potassium ions in the channel. The prominent oscillations seen in the selectivity filter are due to the two resident ions, whose locations are shown in Fig. 8 *B*. Superimposed on the curves are the potential profiles obtained in the absence of ions and protein atom charges (broken lines). These profiles, which are similar to those found in Poisson-Boltzmann solutions (Roux et al., 2000), illustrate that the potential in the pore changes rapidly in the narrow segment of the channel and more slowly in the wider segment.

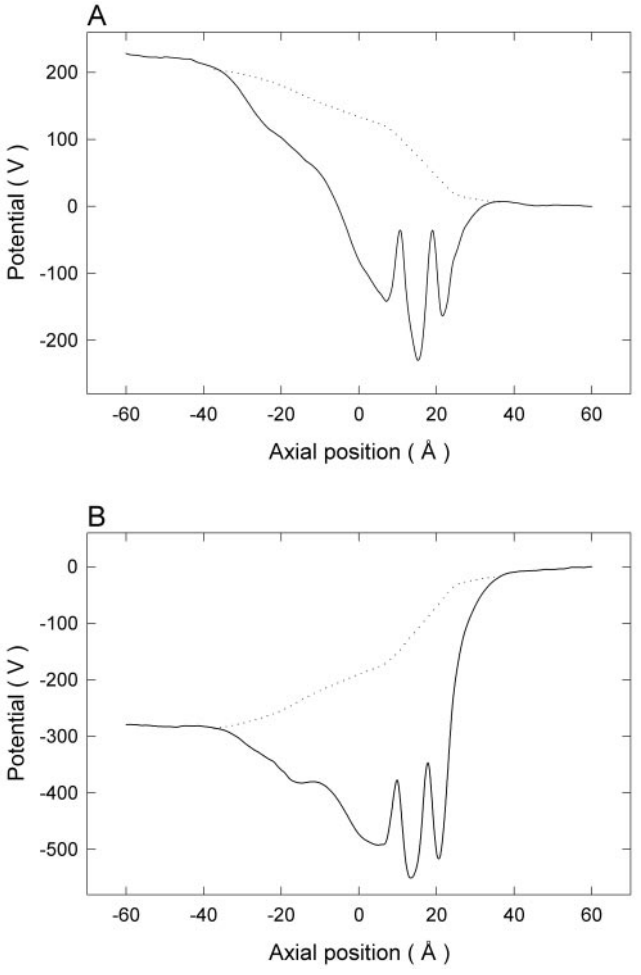

FIGURE 7 The electric potential profiles in the channel with $R_{min} = 4$ Å. The potential along the z axis of the channel is averaged over 10-ns BD simulations and drawn as solid curves. All atomic partial charges in the protein are included, and no restrictions are placed on ionic positions. Uniform electric fields of E_0 (A) and $-E_0$ (B) are applied across the channel to create the potential differences between the centers of the reservoirs (see Table 2). The potential profiles in the absence of protein atomic charges and ions are drawn as dashed curves for comparison.

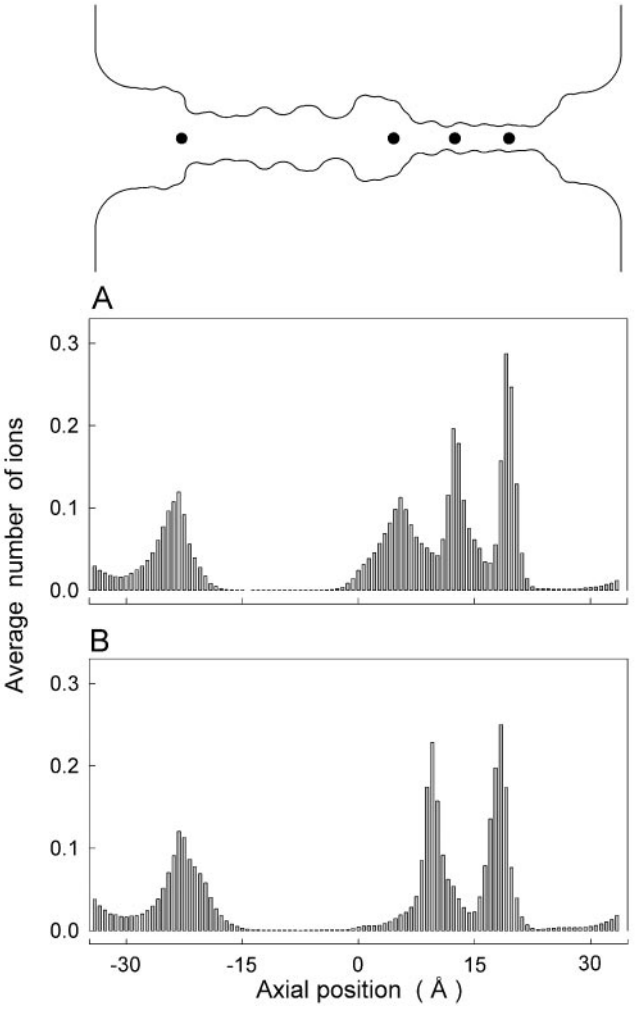

FIGURE 8 Average number of ions in the channel with $R_{min} = 3$ Å with no applied field (A) and with an applied field of $E_0/2$ (B). The channel with $q_i = 0.7e$ is divided into 100 sections, and the average number of ions in each section is calculated over a simulation period (0.1 μs). The outline of the channel and the approximate locations of ions in the absence of an applied field are shown in the inset.

Ions in the channel

In Fig. 8, the histograms of ions in the channel with $R_{min} = 3$ Å are illustrated. To construct the histograms, the channel is divided into 100 thin sections, and the average number of ions over a 0.1-μs simulation is plotted. The concentration of KCl in the reservoirs are kept constant at 300 mM and $q_i = 0.3\,e$. With no applied potential, there are three regions in the selectivity filter and cavity where ions dwell preferentially (Fig. 8 A). The locations of their maxima are $z = 4.5$ Å (inside the cavity), 12.3 Å (near the T_{75} carbonyl oxygen), and 19.2 Å (near the Y_{78} carbonyl oxygen). Also, there is another prominent peak in the histogram, centered at -21 Å, near the E_{118} side chain. The average number of ions is 2.9 in the selectivity filter and the cavity and 0.9 near the intracellular entrance of the channel. The ion in the cavity region tends to reside mostly off-axis, as a result of the strong interaction with the oxygen atoms of the T_{74} residue at the base of the pore helix. These positions are in close agreement with positions observed in Rb^+ x-ray diffraction maps (Doyle et al., 1998). When an electric field E_0 is applied across the channel so that ions steadily move from inside to outside, the pattern of the histogram shifts, as illustrated in Fig. 8 B. There are now two prominent peaks in the selectivity filter region and one peak, as before, in the intracellular entrance of the channel. The average number of ions in the selectivity filter and cavity is now 2.2, whereas that near the intracellular cellular entrance is 1.1. We remark that with charge $q_i = 0.3\,e$ on the intracellular dipoles, the distributions are very similar, except that 1.0 ion resides

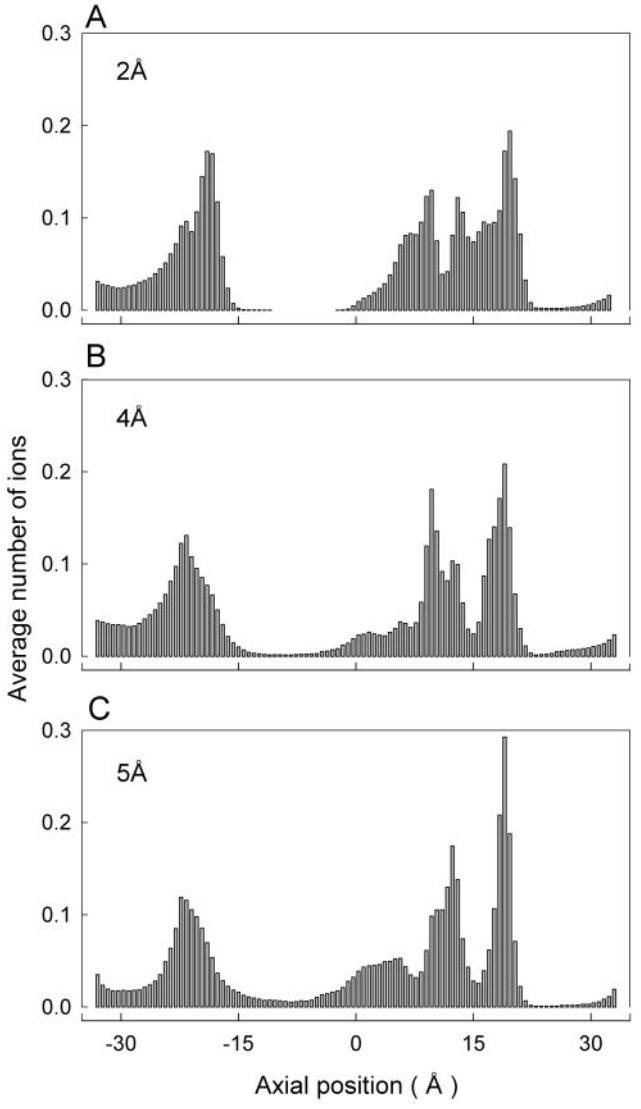

FIGURE 9 Average number of ions with no applied potential for the channels with R_{min} = 2 Å (*A*), 4 Å (*B*), and 5 Å (*C*). For all histograms, $q_i = 0.5e$ is used.

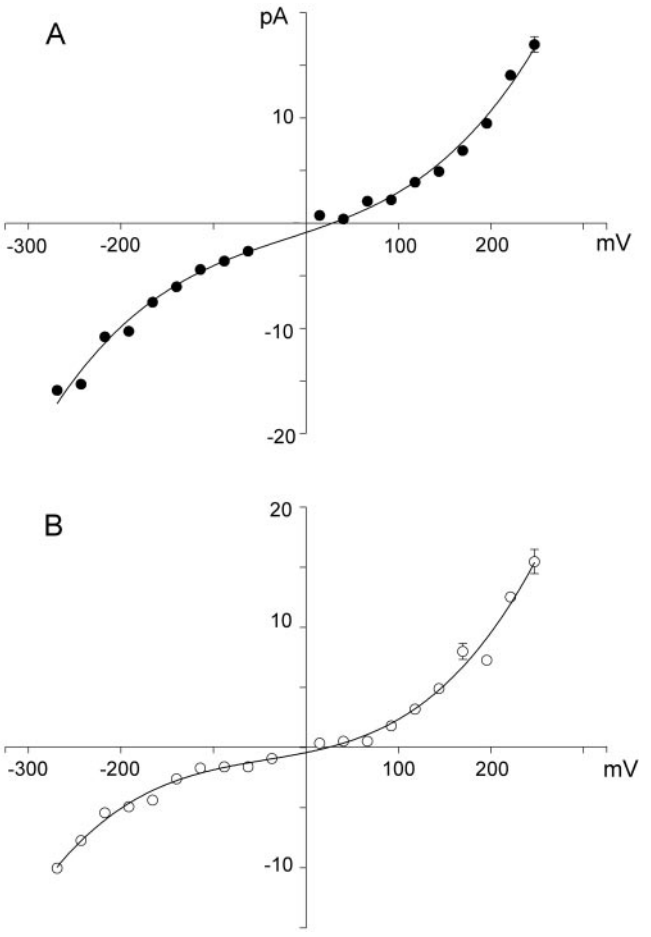

FIGURE 10 Current-voltage relationships for the channel with R_{min} = 3 Å. The magnitude of the current passing through the channel with a symmetric solution of 300 mM KCl in both reservoirs is plotted against the applied potential. The value of q_i placed on the E_{118}/R_{117} residues is 0.7 *e* (*A*) and 0.3 *e* (*B*).

near the intracellular entrance. In Fig. 9, we illustrate three histograms obtained from the channels with R_{min} = 2, 4, and 5 Å with no applied field. All histograms show three distinct peaks in the selectivity filter and the cavity. The average number of ions in the channel is similar in each case, 2.7 in the extracellular side and 1.3 in the intracellular side.

Current-voltage relationships

We study the conductance properties of potassium ions under various conditions by performing BD simulations. The current-voltage curves for the channels with different intra-pore radii are shown in Figs. 10 and 11. For the 3-Å channel, two current-voltage curves are presented, one with q_i = 0.7 *e* (Fig. 10 *A*) and the other with q_i = 0.3 *e* (Fig. 10 *B*). Both curves are fairly linear through the origin when the applied potential is less than ±150 mV, but they deviate systematically from Ohm's law with a further increase in the membrane potential. This nonlinearity results from the presence of an energy barrier in the channel. Intuitively, a barrier is less of an impediment to a permeating ion when the driving force is large. The outward conductance of the channel at an applied potential of 150 mV is 34 ± 4 pS with q_i = 0.3 *e*, and a similar value is obtained for q_i = 0.7 *e*. The inward and outward currents are approximately symmetrical when q_i is 0.7 *e* (Fig. 10 *A*), but the curve becomes pronouncedly asymmetrical when q_i is reduced to 0.3 *e* (Fig. 10 *B*).

The current-voltage curves obtained from the channels with R_{min} = 2, 4, and 5 Å are illustrated in Fig. 11. The features observed in the 3-Å channel are also apparent in the curves shown in Fig. 10. In each of the three curves, there is a systematic deviation from linearity at high applied

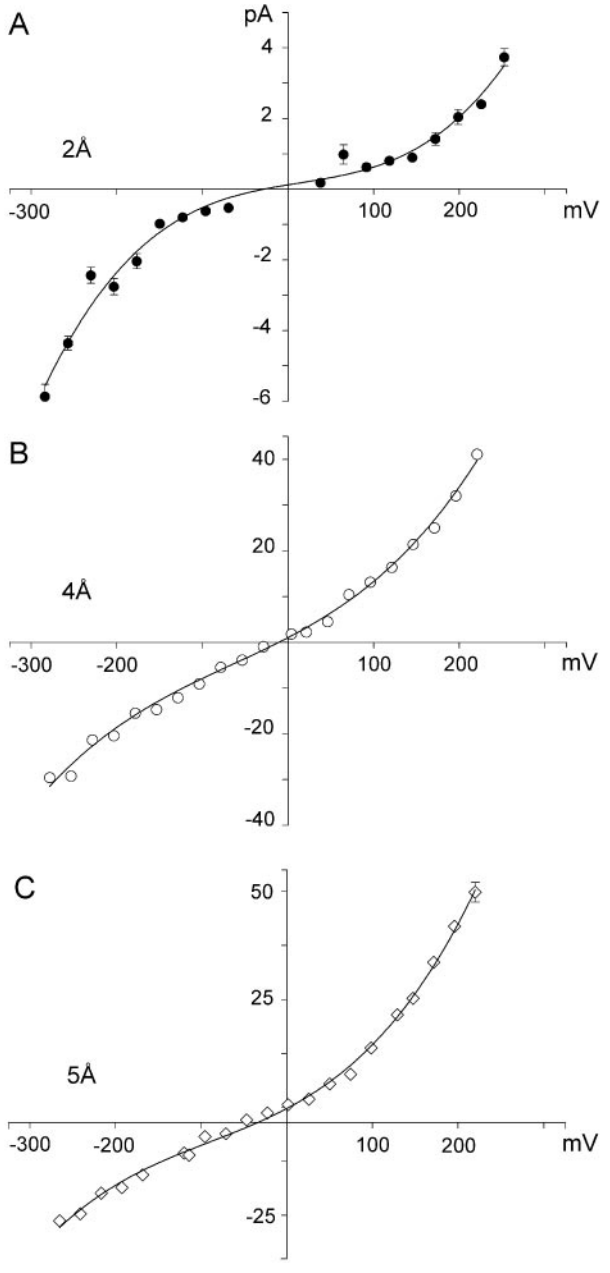

FIGURE 11 Current-voltage relationships for the channels with R_{min} = 2 Å (*A*), 4 Å (*B*), and 5 Å (*C*). The simulation conditions used to generate the data points are the same as in Fig. 10.

potentials, with the degree of nonlinearity being most pronounced in the 2-Å channel. Also, slight asymmetries between the inward and outward currents can be discerned from the curves. The conductances at 150 mV for the channels with R_{min} = 2, 4, and 5 Å are, respectively, 6 ± 2, 147 ± 7, and 172 ± 15 pS. The corresponding values at −150 mV are 7 ± 1, 96 ± 4, and 93 ± 12 pS.

The current-voltage relationships from the KcsA potassium channel have been determined by several groups. The values of the outward conductance at 100 mV they report are 135 pS with 200 mM KCl (Cuello et al., 1998), 97 pS with 250 mM KCl (Meuser et al., 1999), and 83 pS with 100 mM KCl (Heginbotham et al., 1999). Taking concentration dependence into account (see Fig. 16), comparison of these values with the calculated conductances suggest an intrapore radius of R_{min} = 3–4 Å. Note that there are substantial variations in the measured values, and more consistent measurements of the KcsA channel conductance would be desirable to determine the model parameters with more certainty. There are also inconsistencies in the degree of rectification observed in experiments. For example, results of Heginbotham et al. (1999) exhibit a pronounced outward rectification, whereas those of Meuser et al. (1999) show symmetrical inward and outward currents. As both experiments were carried out at similar pH levels, it is difficult to understand the origin of this discrepancy. Our simulations (Fig. 10) suggest that rectification arises from a reduction of charges on the glutamate residues E_{118} as a result of protonation at lower pH levels. Thus, accurate measurement of pH dependence of inward and outward currents would be very valuable in pinpointing the charge state of the E_{118} residues.

Dielectric constant of protein

In the preceding analyses, we used $\varepsilon_p = 2$ for the dielectric constant of protein. Unlike water and lipid, which form homogeneous media, proteins are quite heterogeneous, exhibiting large variations in polarizability depending on location (interior or surface) and nature of the process (for recent reviews, see Nakamura, 1996; Schutz and Warshel, 2001). From a microscopic point of view, this should make assigning a fixed ε_p value to an entire protein in continuum electrostatic calculations problematic, but in practice, it seems to work quite well. In the following series of simulations, we use ε_p = 3.5 and 5 in solving Poisson's equation and compare the results of BD simulations obtained by using these two different values to those obtained by assuming $\varepsilon_p = 2$. We show that the precise value of the dielectric constant of protein we adopt has only negligible effects on the macroscopic properties one derives from BD simulations.

We first compare in Fig. 12 *A* the energy profiles encountered by an ion traversing the channel when ε_p is assumed to be 2 (broken line) and 5 (solid line). In this and the following figures, we use the channel with the R_{min} = 4 Å. The profiles are obtained with two ions placed in the selectivity filter. With 0.5 *e* placed on the E_{118} and R_{117} and an applied field of $+E_0$, the depth of the barrier height V_B encountered by the third ion attempting to proceed toward the inner cavity increases from 2.75 *kT* to 3.37 *kT* as ε_p is changed from 2 to 5. In Fig. 12 B, we show the variation of outward currents under the influence of an applied field of $+E_0$ with the charge placed on the E_{118} and R_{117} residues (filled circles). With $\varepsilon_p = 5$, the peak current is observed

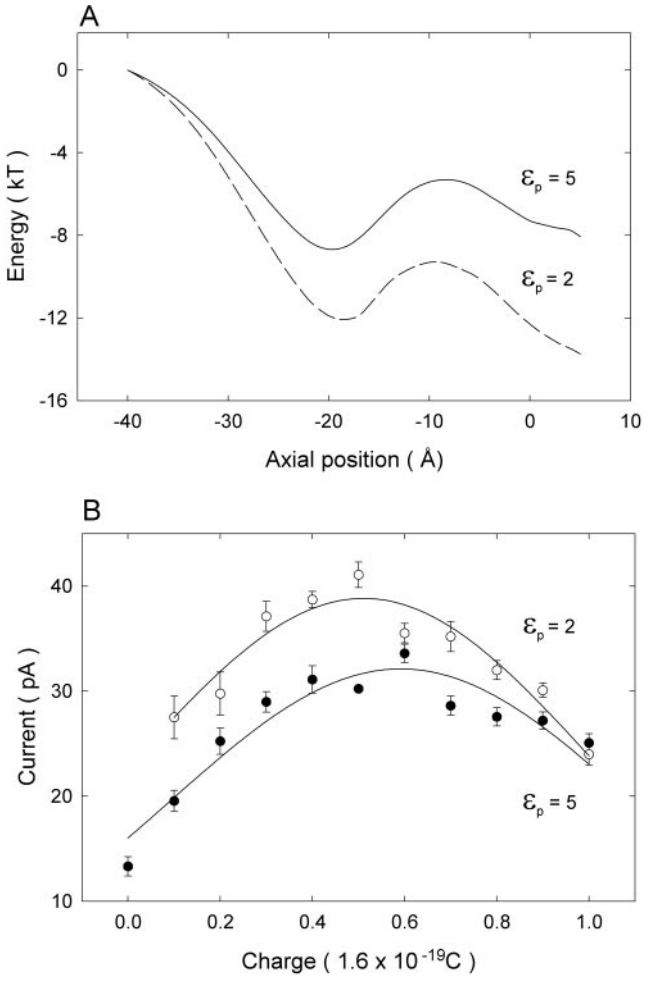

FIGURE 12 Energy profiles and the variation of currents with charges on the glutamate-arginine residues obtained with $\varepsilon_p = 2$ and 5. The field of 2×10^7 V/m is applied. The 4-Å-channel model is used for this and the subsequent two figures (Figs. 13 and 14). (*A*) The profiles are constructed in the presence of two ions in the selectivity filter with $\varepsilon_p = 5$ (——) and $\varepsilon_p = 2$ (— — —). (*B*) The outward current plotted against q_i with $\varepsilon_p = 5$ (●) is compared with that obtained with $\varepsilon_p = 2$ (○), reproduced from Fig. 4 *B*.

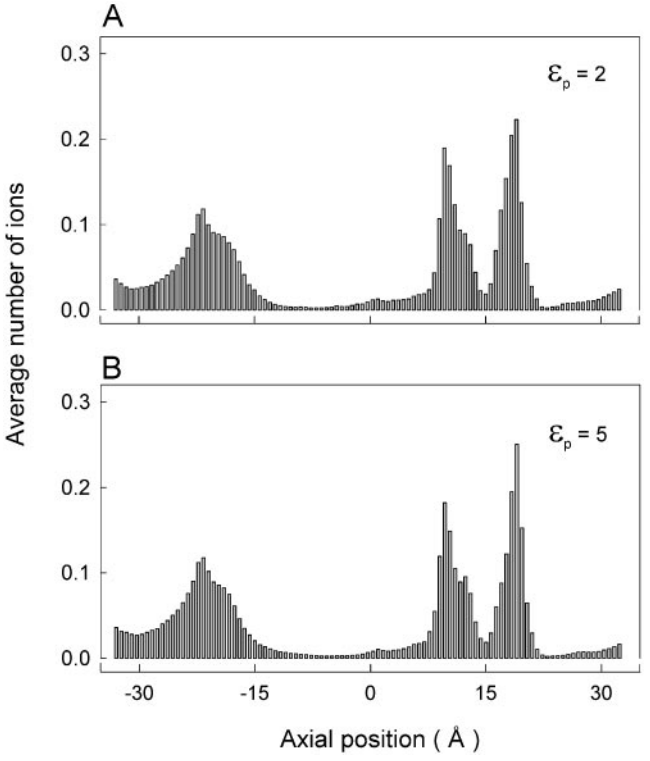

FIGURE 13 Average number of ions in the channel with the assumed values of $\varepsilon_p = 2$ (*A*) and $\varepsilon_p = 5$ (*B*). The histograms are constructed in the presence of an applied field of 2×10^7 V/m.

when the ionizable residues carry 0.6 *e*. Superimposed on the graph are the data for outward currents illustrated in Fig. 4 *B*, where the simulations are carried out with $\varepsilon_p = 2$ (open circles). The current is slightly attenuated when ε_p is increased, and the optimum charge for the glutamate-arginine pairs shifts from 0.5 *e* to 0.6 *e*.

The location and the number of ions in the channel in a conducting state also remain unchanged when ε_p is increased from 2 to 5, as shown in Fig. 13. The histograms are tabulated during the simulation period of 0.1 μs in the presence of an applied field of $+E_0$. The average number of ions in the selectivity filter and inner chamber is 2.23 when $\varepsilon_p = 5$ and 2.33 when $\varepsilon_p = 2$. The corresponding numbers in the intracellular half of the channel are 1.65 and 1.49.

Fig. 14 shows the current-voltage relationships derived by using $\varepsilon_p = 3.5$ and 5.0. Superimposed on these curves is the curve reproduced from Fig. 11 *B* with $\varepsilon_p = 2$. The currents at all driving voltages are slightly attenuated when the ε_p is increased. This decrease is due to a small increase in the height of the energy barrier V_B, as illustrated in Fig. 12 *A*.

There are several microscopic investigations of the dielectric constant of proteins from MD simulations (Smith et al., 1993; Simonson and Perahia, 1995; Simonson and Brooks, 1996; Simonson, 1998; Pitera et al., 2001). The consensus emerging from these MD studies of globular proteins is that the effective dielectric constant for the whole protein varies between 10 and 40 depending on the choice. However, when only the interior region of the protein consisting of the backbone and uncharged residues is considered, ε_p values drop to 2–4. Thus, the relatively large effective ε_p values extracted from MD are mostly due the charged side chains on the protein surface. These studies suggest using a low ε_p value in the protein interior and a transition region between the protein and solvent with a medium ε value that takes into account the polarizable side chains as well as the more ordered layer of water surrounding the protein. Estimating ε_p for proteins forming the channel wall using MD calculations presents an inverse problem. Here, water is embedded in protein rather than

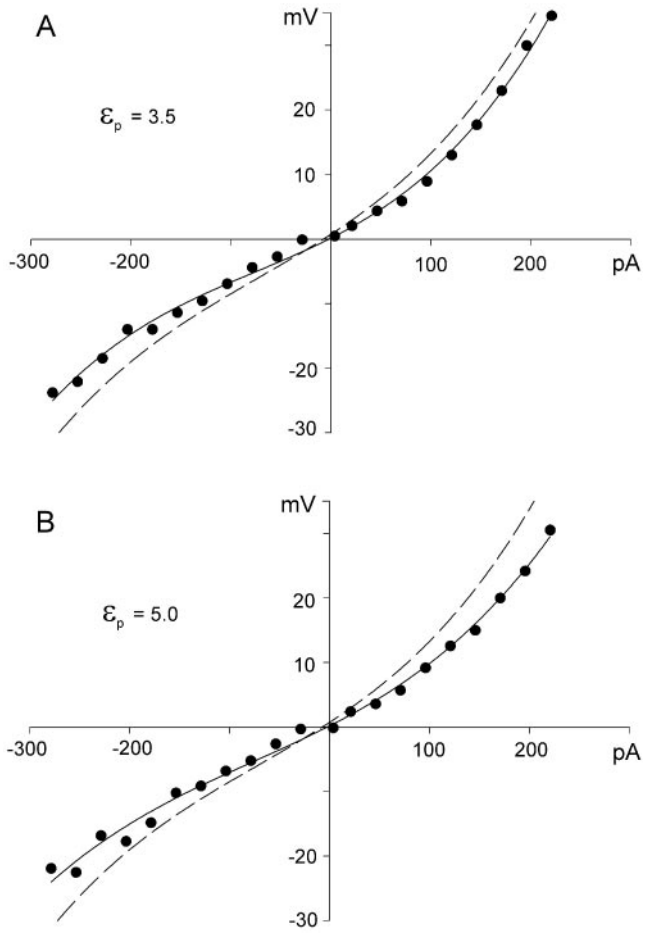

FIGURE 14 Current-voltage relationships derived with $\varepsilon_p = 3.5$ (*A*) and $\varepsilon_p = 5$ (*B*). For comparison, the curve fitted for the current-voltage date illustrated in Fig. 11 *B* is superimposed in *A* and *B* (— — —).

protein embedded in water. Although the quantitative results will certainly be different from globular proteins, we expect the general features mentioned above to apply to the membrane proteins. This issue clearly deserves further MD studies. Our studies, nevertheless, indicate that the calculations carried out using $\varepsilon_p = 2$ remain largely valid even if the effective dielectric constant of channel protein turns out to be substantially higher than 2.

Analyses of conduction processes

In analogy with the flow of a liquid through a constricted pore, one would naively expect that the passage of ions across the narrow selectivity filter is the rate-limiting step for conduction across the potassium channel. Our detailed analysis of conduction process reveals that this is not the case. This is because ions diffuse singly through the intracellular gate and cavity regions but undergo a rapid multi-ion shuttling process within the selectivity filter. We have shown earlier that ionic mobility in the filter region has little impact on conductance because permeation through the filter is governed by the electrostatic repulsion of ions (Chung et al., 1999). These rapid movements of ions in the filter have also been observed in MD studies (Allen et al., 1999); thus, they are not artifacts of using a rigid filter structure in the BD simulations.

We first discuss the potential energy profiles for three K^+ ions in the channel as they provide an intuitive picture for the permeation process. The profiles shown in Fig. 15 *A* are constructed as in Fig. 6 *C*: two ions are placed in the selectivity filter and their positions are varied to minimize their energy as a third ion is moved from $z = -50$ to $z = 10$ Å in 1-Å steps. A driving field of E_0 is applied to move ions outward. It is seen that for permeation to take place, an ion in the energy well near $z = -20$ Å has to go over the barrier at $z = -8$ Å. The height of this barrier V_B, measured as the potential energy difference between $z = -20$ and -8 Å, decreases as the intra-pore radius is increased: $V_B = 11.1$, 6.9, 3.3, and 1.3 kT for $R_{min} = 2$, 3, 4, and 5 Å, respectively (here $q_i = 0.3\ e$ is used for the 3-Å channel). Note that in all cases, once an ion is over the barrier, it is driven toward the selectivity filter under a potential gradient. The Coulomb force exerted by this ion approaching the cavity disrupts the equilibrium of the two resident ions in the filter (see Fig. 8 *B*), resulting in ejection of the outermost ion to the reservoir and thus completing the conduction event.

The profiles encountered by an ion transiting in the inward direction under a driving field of $-E_0$ are similarly constructed and illustrated in Fig. 15 *B*. Here, two ions are placed in the selectivity filter and one ion at the bottom of the energy well near the intracellular entrance. A test ion is then moved from $z = 10$ Å to $z = -50$ Å, while allowing the other three ions to adjust their positions. The barrier heights encountered by the test ion between $z = 8$ and -8 Å are given by $V_B = 7.7$, 4.9, 3.8, and 3.8 kT for $R_{min} = 2$, 3, 4, and 5 Å, respectively. The differences between the inward and outward barriers provide a qualitative explanation for the rectification of the *I-V* curves observed in Figs. 10 and 11. For example, the substantial outward rectification seen in the 5-Å channel (Fig. 11 *C*) arises from the outward barrier being three times smaller than the inward one.

From these profiles, we expect that an ion attempting to climb over the barrier to move more slowly and spend more time in the deeper wells compared with shallower ones, thus giving a simple explanation for the rapid increase in conductance with radius seen in Figs. 10 and 11. We quantify the above statement through an analysis of the ion trajectories obtained from BD simulations. For reference, we note that the drift velocity of potassium ions in a bulk solution under a driving field of $E_0 = 2 \times 10^7$ V/m is 1.5 m/s. The average drift velocity of ions in the channel as they climb up the energy barrier in Fig. 15 is found to be substantially smaller than the drift velocity in a bulk solution, but it becomes larger than the bulk value once they are over the

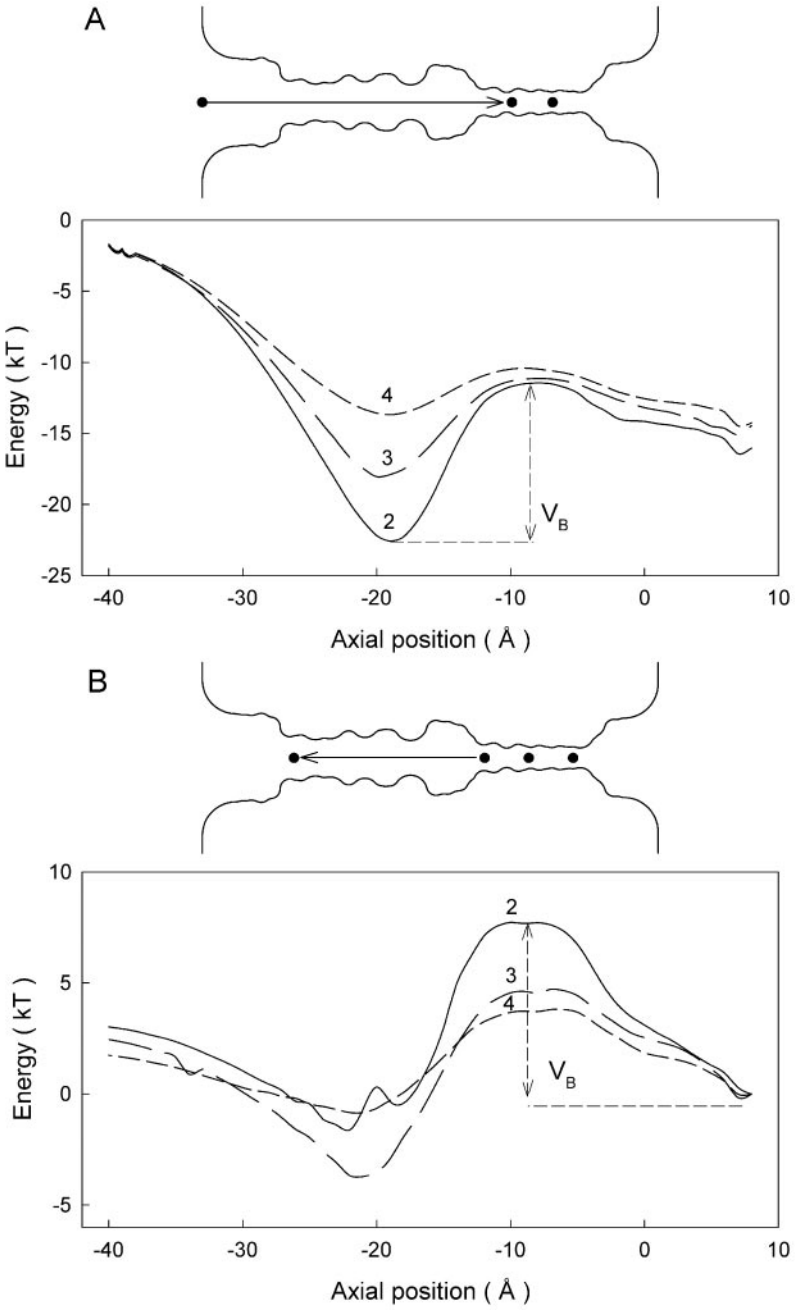

FIGURE 15 Rate-limiting steps for ion permeation. (*A*) The energy profiles presented to a potassium ion as it proceeds toward the cavity from inside the cell are plotted. A schematic diagram in the inset shows the location of two resident ions in the selectivity filter when the permeating ion is at $z = 0$ Å. The numbers accompanying the profiles indicate the intra-pore radius of the channel. The ion traversing the 2-Å channel, for example, must overcome the barrier whose height is indicated as V_B. (*B*) The potential profiles presented to the innermost ion in the selectivity filter as it moves toward the intracellular space are plotted. The three profiles correspond to channels with $R_{min} = 2$, 3, and 4 Å. The barrier height for the 2-Å channel is indicated as V_B. In the inset, the positions of the resident ions and the test ion at its starting point are indicated. The profiles obtained from the 5-Å channel, not shown here for clarity, are similar to that obtained from the 4-Å channel.

barrier and move toward the cavity. For example, for the 2-Å channel, the respective velocities before and after the barrier are 0.24 and 5.73 m/s under the driving field of E_0. Thus, once an ion climbs over the energy well, the transit across the remaining part of the pore is rapid. As the channel gets larger, the barrier becomes less steep and the drift velocities on either side of the barrier gradually approach toward the bulk value. Here, velocities are determined by averaging the ionic speeds during conduction processes whenever there is an ion in the desired segment.

The time an ion spends in various parts of the channel also provides valuable insights into the permeation process. The maximum number of ions the channel can process is expected to be determined primarily by the time it takes for an ion to climb out of the well located near $z = -20$ Å. In Table 4, we tabulate the average time the well remains empty (t_0) and occupied (t_1) by an ion for the four channels with different intra-pore radii. The mean transit time is essentially the sum of the times t_0 and t_1. The waiting times shown in Table 4 correlate well with the barrier heights (Fig. 15), clearly demonstrating that the rate-limiting step for conduction is passing of the ions over the central barrier. For the most part, an ion resident in the well makes repeated attempts to move toward the cavity, but success is rare and

TABLE 4 Average time that the well near $z = -20$ Å is empty (t_0) and occupied by an ion (t_1), per conduction event, are tabulated for the driving field of E_0

R_{min} (Å)	t_0 (ns)	t_1 (ns)
2	0.4 ± 0.1*	45.1 ± 3.7
3	0.5 ± 0.1	8.5 ± 0.6
4	0.7 ± 0.1	3.2 ± 0.2
5	0.4 ± 0.1	2.2 ± 0.2

*Times are ±1 SEM.

is proportional to the barrier height. Analysis of BD trajectories reveals that, under the applied field of E_0, the success rates are 1.5%, 4%, and 5.8% for the 3-, 4-, and 5-Å channels, respectively.

Saturation of channel currents

Experimentally, the current I across the potassium channel first increases with an increasing ionic concentration [K] and then saturates, leading to a current-concentration relationship of the Michaelis-Menten form:

$$I = \frac{I_{max}}{1 + K_s/[K]}, \quad (4)$$

which shows that the current approaches the saturation current I_{max} when $[K] \gg K_s$. Theoretically, the conductance-concentration curve is expected to saturate if the transport of ions across the channel is determined by two independent processes, one of which depends on ionic concentrations on the two sides of the channel and one that does not (Chung et al., 1999).

In Fig. 16, the current obtained from BD simulations is plotted against the concentrations of potassium ions in the reservoirs. The four sets of curves in Fig. 16 *A* represent the outward currents obtained from the channel with $R_{min} = 2$, 3, 4, and 5 Å under the applied field of E_0. The inward currents (Fig. 16 *B*) are obtained similarly by reversing the applied field to $-E_0$. The curve for the 4-Å channel in Fig. 16 *B* overlaps with that of the 5-Å channel. For clarity it is omitted and instead shown in the following figure. The solid lines fitted through the data points are calculated from Eq. 4 and have the same shape as those observed experimentally. The values of K_s used to fit the data for the outward currents of the $R_{min} = 2$-, 3-, 4-, and 5-Å channels are 113 ± 29, 135 ± 8, 277 ± 54, and 282 ± 46 mM, respectively. These half-saturation values are shown in the figure as shaded diamonds. The corresponding K_s values for the inward currents are 50 ± 16, 170 ± 22, 1894 ± 1182, and 1790 ± 839 mM, respectively. For both outward and inward currents, the half-saturation points tend to shift toward higher concentrations as the radius of the channel is increased. This result follows directly from the reduction of the central barrier with increasing radius (Fig. 15) and the concomitant decrease in waiting times in the intra-pore energy well (Table 4). Simply put, ions are processed through the channel faster as the intra-pore radius gets larger.

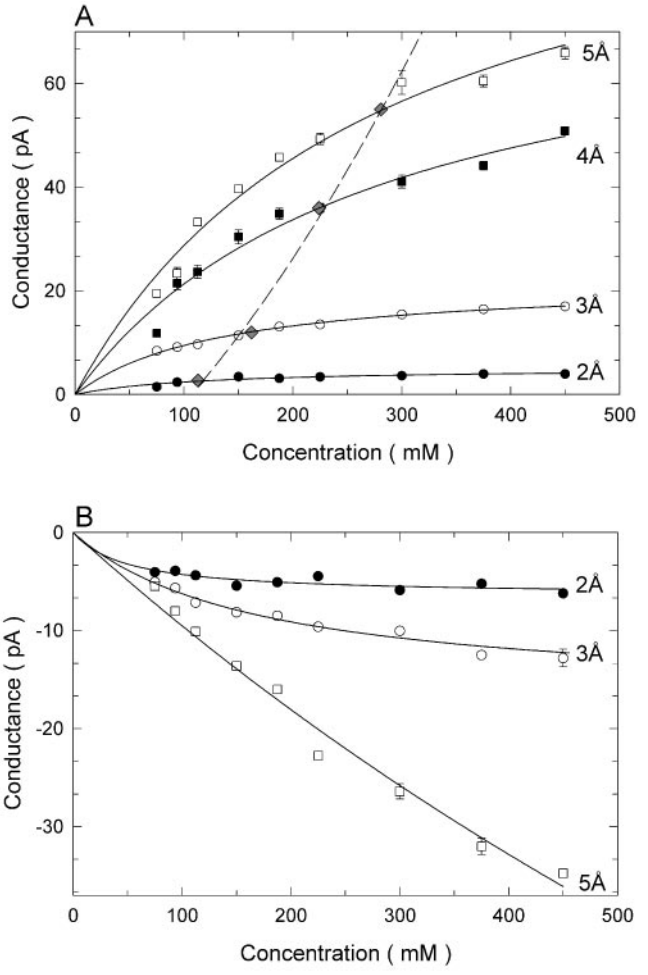

FIGURE 16 Current-concentration relationships for channels of various size. The outward (*A*) and inward (*B*) currents are obtained with symmetrical solutions of varying concentrations KCl in the reservoirs. The data points are fitted by the solid line using Eq. 4. The half-saturation points K_s used to fit the data points for the outward currents are indicated with shaded diamonds.

The concentrations for half-maximum current we derive are slightly higher than the experimentally determined values for potassium channels (Coronado et al., 1980; Rae et al., 1988). Because these are not for the KcsA channel, a direct comparison is not possible. Our K_s values also depend to a small extent on the strength of driving force used to generate the current. In Fig. 17, we plot the current-concentration curves for the 4-Å channel, using five different driving fields increasing from $E_0/5$ to E_0 in equal steps (the corresponding potential differences are indicated next to each curve). The K_s values for the outward currents (Fig. 17 *A*) are all in the range of 250–300 mM. When the applied field is reversed, the estimated K_s values are more spread (300–450 mM), except for the applied potential of 280 mV

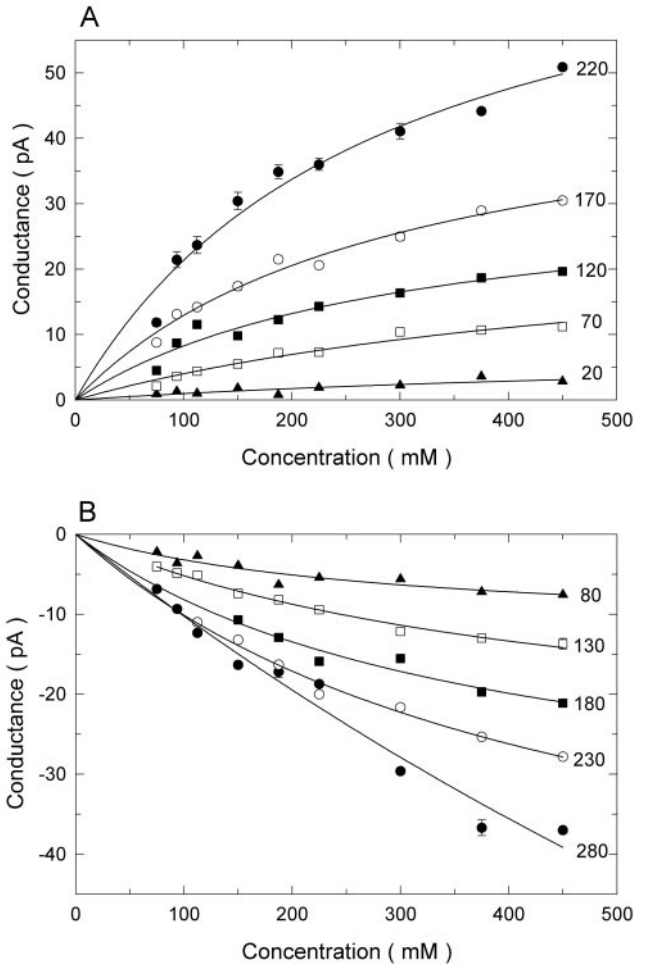

FIGURE 17 The effect of applied potential on current-concentration relationships for R_{min} = 4 Å. The outward (*A*) and inward (*B*) currents generated by five different applied potentials (given next to the each curve) are plotted against ionic concentrations in the reservoirs. The data points are fitted by the solid line using Eq. 4.

where the data points are too noisy to extract a meaningful K_s value.

CONCLUDING REMARKS

In this study, we first construct several open-state KcsA channels following modeling with MD simulations and then perform BD simulations using these models that include the full experimentally determined protein. To render the channel permeable to ions, the narrow intracellular hydrophobic pore deduced from the crystallographic structure needs to be widened by at least 1 Å. Experimentally, the current across some potassium channels is large, reaching ~25 pA at an applied potential of 100 mV (Farley and Rudy, 1998; Ikemoto et al., 1989), whereas the current across small potassium channels can be nearly two orders of magnitude smaller (Hille, 1992; Hirschberg et al., 1999). Such a large range of channel conductance is observed when the minimum radius of the pore entrance facing the intracellular space is increased from 2 Å to 5 Å. Although this result is obtained using the KcsA structure, all potassium channels share a common feature of being highly selective to potassium ions and display broadly similar selectivity sequences and relative permeability ratios for monovalent cations. The amino acid sequence of the peptide chains lining the selectivity filter of all potassium channels is known to be highly conserved. Thus it is possible that the diversity of potassium channels results from structural changes on the protein architecture near the intracellular segment of the pore.

For optimum conduction, the charge on the glutamic acid residues lining the pore near the intracellular entrance (E_{118}) must be reduced from the fully ionized form to less than 0.8 *e*, possibly by a decrease in electrolyte pH inside the cell. The conductance depends critically upon the charge on these glutamate-arginine (E_{118}/R_{117}) residues when it is narrow but becomes relatively insensitive to this charge when it is wide. For the channel with 3-Å radius, a change in the protonation states of ionizable residues near the channel entrances is seen to lead to subtle differences in the shape of the current-voltage curve, current-concentration curve, and ionic distribution within the channel. Once accurate single-channel measurements become available, the results of these simulations can be used to deduce the most likely protonation states of these ionizable side chains, as well as the aperture of the intra-pore entrance in the conducting state.

Analysis of energy profiles shows that the channel in the absence of an external field can house three ions in the selectivity filter-cavity region. When an external field is applied, the three-ion system is destabilized such that it houses only two ions on average. The permeation process is essentially governed by the central barrier whose height depends on the intra-pore radius. Broadly similar features were observed in the earlier BD study with a simplified model of the KcsA channel (Chung et al., 1999).

Using microscopic and semi-microscopic approaches, we have deduced some of the salient properties of the KcsA potassium channel that can be measured experimentally using patch-clamp techniques. The parameters featured in our model can be further refined to better predict experimental quantities. We make a set of testable predictions. First, the *I-V* curves for potassium channels, especially those with small conductance levels, should be approximately linear when the applied potential is less than 150 mV but deviate from Ohm's law with a further increase in the membrane potential. Second, the half-saturation value in the conductance-concentration relationship, obtained from a fit to the Michaelis-Menten form, tends to increase with an increasing driving force. Similarly, currents in potassium channels with high-conductance levels are expected to saturate more slowly than those with low-conductance levels. Third, the magnitude of current flowing across the channel

depends on the intracellular pH, because the ring of acidic residues guarding the intracellular gate plays a role in controlling conductance. We predict that this pH dependence of conductance will be pronounced for small potassium channels and negligible for large potassium channels. Finally, there is an intriguing possibility that conductance substates of a single channel may arise from changing protonation states of the ionizable residues, such as the E_{118} in the KcsA potassium channel. If the effective charge carried by this residue in a 4-Å channel, for example, fluctuates from 0.5 *e* to fully neutral in the course of an open episode, we expect the current to drop from the fully open level to a partially open level, which will be about one-half in amplitude of the fully open state. It will be useful to construct *I-V* curves and current-concentration curves from the fully open state and subconductance states from single-channel recordings. If sublevels observed in patch-clamp recordings indeed arise from the mechanisms we postulate here, then the shapes of these curves derived from the fully open state should be pronouncedly different from those derived from one of the substates.

REFERENCES

Allen, T. W., A. Bliznyuk, A. P. Rendell, S. Kuyucak, and S. H. Chung. 2000a. The potassium channel: structure, selectivity and diffusion. *J. Chem. Phys.* 112:8191–8204.

Allen, T. W., S. Kuyucak, and S. H. Chung. 1999. Molecular dynamics study of the KcsA potassium channel. *Biophys. J.* 77:2502–2516.

Allen, T. W., S. Kuyucak, and S. H. Chung. 2000b. Molecular dynamics estimates of ion diffusion in model hydrophobic and the KcsA potassium channels. *Biophys. Chem.* 86:1–14.

Åqvist, J., and V. Luzhkov. 2000. Ion permeation mechanism of the potassium channel. *Nature.* 404:881–884.

Bernèche, S., and B. Roux. 2000. Molecular dynamics of the KcsA K^+ channel in a bilayer membrane. *Biophys. J.* 78:2900–2917.

Biggin, P. C., G. R. Smith, I. Shrivastava, S. Choe, and M. S. P. Sansom. 2001. Potassium and sodium ions in a potassium channel studied by molecular dynamics simulations. *Biochim. Biophys. Acta.* 1510:1–9.

Bockris, J. O'M., and A. K. N. Reddy. 1970. Modern Electrochemistry, Vol. 1. Plenum, New York.

Brooks, B. R., R. E. Bruccoleri, B. D. Olafson, D. J. States, S. Swaminathan, and M. Karplus. 1983. CHARMM: a program for macromolecular energy, minimization, and dynamics calculations. *J. Comp. Chem.* 4:187–217.

Chung, S. H., T. W. Allen, M. Hoyles, and S. Kuyucak. 1999. Permeation of ions across the potassium channel: Brownian dynamics studies. *Biophys. J.* 77:2517–2533.

Chung, S. H., M. Hoyles, T. W. Allen, and S. Kuyucak. 1998. Study of ionic currents across a model membrane channel using Brownian dynamics. *Biophys. J.* 75:793–809.

Coronado, R., R. L. Rosenberg, and C. Miller. 1980. Ionic selectivity, saturation, and block in a K^+-selective channel from sarcoplasmic reticulum. *J. Gen. Physiol.* 76:425–446.

Corry, B., T. W. Allen, S. Kuyucak, and S. H. Chung. 2001. Mechanisms of permeation and selectivity in calcium channel. *Biophys. J.* 80: 194–214.

Cuello, L. G., J. G. Romero, D. M. Cortes, and E. Perozo. 1998. pH dependent gating in the *Streptomyces lividans* K^+ channel. *Biochemistry.* 37:3229–3236.

Doyle, D. A., J. M. Cabral, R. A. Pfuetzner, A. Kuo, J. M. Gulbis, S. L. Cohen, B. T. Chait, and R. MacKinnon. 1998. The structure of the potassium channel: molecular basis of K^+ conduction and selectivity. *Science.* 280:69–77.

Farley, J., and B. Rudy. 1988. Multiple types of voltage-dependent Ca^2-activated K^+ channels of large conductance in rat brain synaptosomal membranes. *Biophys. J.* 53:919–934.

Guidoni, L., V. Torre, and P. Carloni. 1999. Potassium and sodium binding to the outer mouth of the K^+ channel. *Biochemistry.* 38:8599–8604.

Guidoni, L., V. Torre, and P. Carloni. 2000. Water and potassium dynamics inside the KcsA K^+ channel. *FEBS Lett.* 477:37–42.

Heginbotham, L., M. LeMasurier, L. Kolmakova-Partensky, and C. Miller. 1999. Single *Streptomyces lividans* K^+ channels: functional asymmetries and sidedness of proton activation. *J. Gen. Physiol.* 114:551–559.

Hille, B. 1992. Ionic Channels of Excitable Membranes, 2nd ed. Sinauer Associates, Sunderland, MA.

Hirschberg, B., J. Maylie, J. P. Adelman, and N. V. Marrion. 1999. Gating properties of single SK channels in hippocampal CA1 pyramidal neurons. *Biophys. J.* 77:1905–1913.

Hoyles, M., S. Kuyucak, and S. H. Chung. 1996. Energy barrier presented to ions by the vestibule of the biological membrane channel. *Biophys. J.* 70:1628–1642.

Hoyles, M., S. Kuyucak, and S. H. Chung. 1998a. Computer simulation of ion conductance in membrane channels. *Phys. Rev. E.* 58:3654–3661.

Hoyles, M., S. Kuyucak, and S. H. Chung. 1998b. Solutions of Poisson's equation in channel-like geometries. *Comput. Phys. Commun.* 115: 45–68.

Ikemoto, Y., K. Ono, A. Yoshida, and N. Akaike. 1989. Delayed activation of large-conductance Ca^{2+}-activated K channels in hippocampal neurons of the rat. *Biophys. J.* 56:207–212.

Lazaridis, T., and M. Karplus. 1999. Effective energy function for proteins in solution. *Proteins.* 35:133–152.

Li, S. C., M. Hoyles, S. Kuyucak, and S. H. Chung. 1998. Brownian dynamics study of ion transport in the vestibule of membrane channels. *Biophys. J.* 74:37–47.

Lide, D. R., Editor. 1994. CRC Handbook of Chemistry and Physics. CRC Press, Cleveland, OH.

Luzhkov, V. B., and J. Åqvist. 2000. A computational study of ion binding and protonation states in the KcsA potassium channel. *Biochim. Biophys. Acta.* 1481:360–370.

Meuser, D., H. Splitt, R. Wagner, and H. Schrempf. 1999. Exploring the open pore of the potassium channel from *Streptomyces lividans. FEBS Lett.* 462:447–452.

Nakamura, H. 1996. Roles of electrostatic interactions in proteins. *Q. Rev. Biophys.* 29:1–90.

Nina, M., D. Beglov, and B. Roux. 1997. Atomic radii for continuum electrostatics calculations based on molecular dynamics free energy simulations. *J. Phys. Chem. B.* 101:5239–5248.

Perozo, E., D. M. Cortes, and L. G. Cuello. 1998. Three-dimensional architecture and gating mechanism of a K^+ channel studied by EPR spectroscopy. *Nat. Struct. Biol.* 5:459–469.

Perozo, E., D. M. Cortes, and L. G. Cuello. 1999. Structural rearrangements underlying K^+-channel activation gating. *Science.* 285:73–78.

Pitera, J. W., M. Falta, and W. F. van Gunsteren. 2001. Dielectric properties of proteins from simulation: the effects of solvent, ligands, pH, and temperature. *Biophys. J.* 80:2546–2555.

Rae, J. L., R. A. Levis, and R. S. Eisenberg. 1988. Ionic channels in ocular epithelia. *In* Ion Channels, Vol. 1. T. Narahashi, editor. Plenum Press, New York. 283–327.

Ranatunga, K. M., I. H. Shrivastava, G. R. Smith, and M. S. P. Sansom. 2001. Side-chain ionization states in a potassium channel. *Biophys. J.* 80:1210–1219.

Roux, B., S. Bernèche, and W. Im. 2000. Ion channels, permeation, and electrostatics: insight into the function of KcsA. *Biochemistry.* 39: 13295–13306.

Sansom, M. S. P., G. R. Smith, C. Adcock, and P. C. Biggin. 1997. The dielectric properties of water within model transbilayer pores. *Biophys. J.* 73:2404–2415.

Schutz, C. N., and A. Warshel. 2001. What are the dielectric "constants" of proteins and how to validate electrostatic models? *Proteins.* 44: 400–417.

Shrivastava, I. H., and M. S. P. Sansom. 2000. Simulation of ion permeation through a potassium channel: molecular dynamics of KcsA in a phospholipid bilayer. *Biophys. J.* 78:557–570.

Simonson, T. 1998. Dielectric constant of cytochrome c from simulations in a water droplet including all electrostatic interactions. *J. Am. Chem. Soc.* 120:4875–4876.

Simonson, T., and C. L. Brooks, III. 1996. Charge screening and the dielectric constant of proteins: insights from molecular dynamics. *J. Am. Chem. Soc.* 118:8452–8458.

Simonson, T., and D. Perahia. 1995. Internal and interfacial dielectric properties of cytochrome c from molecular dynamics in aqueous solution. *Proc. Natl. Acad. Sci. U.S.A.* 92:1082–1086.

Smith, P. E., R. M. Brunne, A. E. Mark, and W. F. van Gunsteren. 1993. Dielectric properties of trypsin inhibitor and lysozyme calculated from molecular dynamics simulations. *J. Phys. Chem.* 97: 2009–2014.

van Gunsteren, W. F., and H. J. C. Berendsen. 1982. Algorithms for Brownian dynamics. *Mol. Phys.* 45:637–647.